Inorganic Chemistry

pubs.acs.org/IC

Article

Single-Source Precursors for the Controlled Aqueous Synthesis of Bismuth Oxyhalides

Matthew N. Gordon, Yanyao Liu, M. Kevin Brown, and Sara E. Skrabalak*

Cite This: *Inorg. Chem.* 2023, 62, 9640−9648

Read Online

ACCESS | Metrics & More | Article Recommendations | Supporting Information

ABSTRACT: Bismuth oxyhalides are a promising class of photocatalysts for harvesting solar energy. These materials are often synthesized in aqueous media with poor synthetic control resulting from the extremely fast nucleation and growth rates of the particles. These fast rates are caused by the rapid precipitation of bismuth salts with free halide ions. We have developed water-soluble precursors combining bismuth with either chlorine or bromine atoms in the same metal−organic complex. With the application of heat, halide ions are released, which then precipitate with bismuth ions as BiOX (X = Cl, Br). By controlling the halide ion formation rate, the nucleation and growth rates of BiOX materials can be tuned to provide synthetic control. The diverse potential of these precursors is demonstrated by synthesizing BiOX in three ways: aqueous colloidal synthesis, solid-state decomposition, and fabrication of films of BiOX via spray pyrolysis of the aqueous precursor solutions. These broadly applicable single-source precursors will enhance the ability to synthesize future BiOX materials with controlled morphologies.

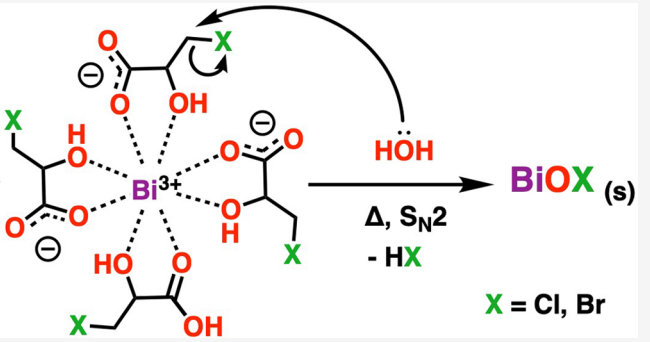

INTRODUCTION

Solar water splitting is a promising platform to generate hydrogen as a clean fuel.[1−10] Bismuth oxyhalides of the form BiOX (X = Cl, Br, I) are a special class of layered photocatalytic materials for this purpose.[11−17] The BiOX crystal structure comprises alternating positively charged $Bi_2O_2^{2+}$ and negatively charged X^- double layers.[18,19] This structure supports their use as photocatalysts, as a static internal electric field is generated between the layers that spatially separates photogenerated holes and electrons, providing a 2-dimensional path to the surface for these charge carriers to engage in redox reactions.

Bismuth oxyhalides can be synthesized easily through the aqueous combination of bismuth and halide sources.[20−24] As an example, Xu and co-workers added an aqueous NaCl solution dropwise to a solution of bismuth nitrate in water/mannitol to form BiOCl nanoplates, which were then annealed.[24] Such hydrolysis-based precipitation reactions, however, are so fast that controlling the nucleation and growth rates of BiOX materials remains challenging. Summarizing this topic, Li, Yu, and Zhang wrote, *"The great challenge for the preparation of well-defined structures is the fast nucleation rate of BiOX in aqueous solutions. As the chemical reaction between $(Bi_2O_2)^{2+}$ cations and X^- anions is very fast, controlling the formation rate of X−Bi−O−Bi−X nucleation is the key to achieve the desired 2-D building blocks."*[14] Other researchers have worked around this problem with creative ways to combine bismuth and halide ions such as combining Bi-containing reverse microemulsions with halide analogues[25] or adding NH_4X salts to a bismuth-based metal−organic framework.[26] Bismuth halide complexes have been previously developed; however, these are only relevant for nonaqueous systems.[27−29] We tackle this challenge here through the design of water-soluble single-source molecular precursors that release halide ions with the application of heat. By controlling the temperature, the rate of X^- generated in solution can be slowed and thus the formation rate of BiOX can be controlled.

Single-source precursors (SSPs) are defined as solitary species that contain all the elements required for a synthetic reaction.[30−37] In our case, a SSP for BiOX would contain Bi, O, and X within one species. SSPs have broad applications, including chemical vapor deposition of films, intermetallic nanoparticle synthesis, and industrial manufacturing of complex metal oxides and chalcogenides.[38−40] The benefits of SSPs over their multisource counterparts include improved homogeneity, stoichiometric control, no differences in precursor rates of vaporization, reaction, or nucleation, and

Received: April 6, 2023
Published: June 2, 2023

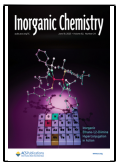

https://doi.org/10.1021/acs.inorgchem.3c01114
Inorg. Chem. 2023, 62, 9640−9648

Scheme 1. Representative Synthesis of BiXLac Complexes and Reaction of Aqueous Complexes with Water at Elevated Temperatures to Form BiOX (s)

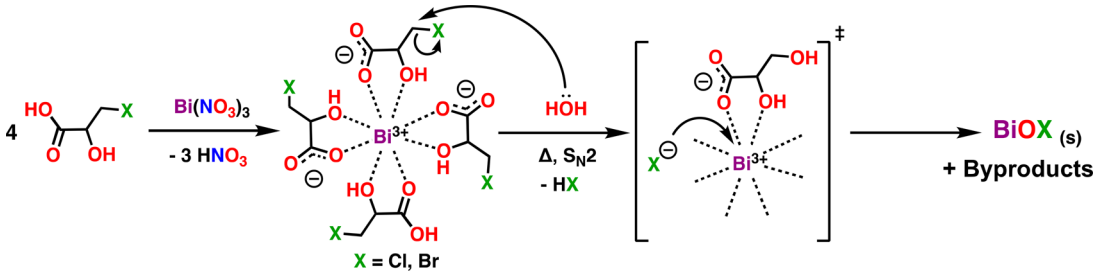

most importantly to us, the molecular combination of incompatible functional groups.[31,41,42]

Previously, we published a synthetic route to BiOX materials using a bismuth lactate complex (one of the few water-soluble bismuth complexes) and an organohalide molecule (organic small molecule containing chlorine or bromine atoms that is water-soluble, including 2-chloroethanol or bromoacetic acid as examples).[43] The bismuth lactate complex served as a method to solubilize Bi^{3+} ions without the hydrolysis that occurs with all common bismuth salts or the need for the use of strongly acidic solutions. The mechanism of BiOX formation is thought to be a nucleophilic substitution reaction between water and the organohalide, releasing the halogen as a halide ion, based on previous NMR evidence. A key factor was the presence of Bi^{3+} serving as a halide scavenger (to form BiOX), thus driving the unfavorable equilibrium toward the production of halide ions. Other potential mechanistic considerations include Bi^{3+} in the complex acting as a Lewis acid to enhance the substitution and/or anchimeric assistance from the adjacent −OH. Regardless of how the halide is removed exactly, because the forward reaction rate is temperature dependent, the control of temperature becomes a synthetic lever to regulate the formation rate of BiOX.

Here, we combine the organohalide functionality directly onto the bismuth lactate complex, forming single-source precursors: bismuth 3-halolactate metal−organic adducts. The crystal structures of both tris(3-chloro-2-hydroxypropanoate)mono(3-chloro-2-hydroxypropanoic acid)bismuth(III), which will be referred to as "BiClLac", and tris(3-bromo-2-hydroxypropanoate)mono(3-bromo-2-hydroxypropanoic acid)bismuth(III), which will be referred to as "BiBrLac," have been solved. These BiXLac (X = Cl, Br) species serve as SSPs to BiOX materials, which is demonstrated in three ways: aqueous colloidal synthesis, solid-state decomposition, and fabrication of films of BiOX via spray pyrolysis of the aqueous precursor solutions. Through this work, a new class of aqueous SSPs toward bismuth oxyhalides is established, with controlled nucleation and growth rates of BiOX for diverse synthetic control.

EXPERIMENTAL SECTION

Materials. Bismuth nitrate pentahydrate (98%), sodium cyanoborohydride (95%), and (±)-3-chloropropane-1,2-diol (98%) were purchased from Alfa Aesar. Ethyl bromopyruvate (96%) was obtained from Ambeed. Nitric acid (ACS Plus) and ethyl acetate (ACS) were purchased from Fisher. Chloroform (ACS) and methanol (ACS, anhydrous) were obtained from Macron. NaCl (≥99.0%) was purchased from VWR. $MgSO_4$ (≥98.0%, anhydrous) was obtained from EMD Millipore. D_2O (99.9 atom % D) was obtained from Sigma-Aldrich. All chemicals were used as received. Milli-Q (18.2 MΩ cm at 25 °C) purified water was used for all experiments, except where D_2O is noted.

Synthesis of 3-Chlorolactic Acid. The synthesis of 3-chlorolactic acid has been fully described in our previous publication.[44] Briefly, (±)-3-chloropropane-1,2-diol was placed in a round-bottom flask. Concentrated nitric acid was added with stirring. (*CAUTION! Handling large amounts of concentrated acids is dangerous, and the reaction produces NO_x gases. For these reasons, it is critical to perform these steps in a fume hood.*) A condenser was attached, and the flask was heated slowly with stirring to 80 °C until a vigorous reaction started. The reaction mixture was kept at 80 °C for 30 min and then raised to 100 °C for another 30 min. The solution was cooled and then neutralized. The product was extracted using ethyl acetate, washed with brine, dried over $MgSO_4$, and concentrated. Chloroform was added to the crude product and kept at −20 °C overnight to produce 3-chlorolactic acid. Fourier-transform infrared spectroscopy (FTIR), ^{1}H nuclear magnetic resonance spectroscopy (NMR), high-resolution mass spectrometry (HRMS), and melting point match previous results (Figure S1).[44]

Synthesis of Ethyl 3-Bromolactate. The synthesis of ethyl 3-bromolactate is adapted from a literature procedure.[45] Briefly, $NaBH_3CN$ (1.45 g, 23.1 mmol) was added to a solution of ethyl bromopyruvate (4.50 g, 23.1 mmol) in methanol (70 mL) and stirred for 1 h at 0 °C. Ethyl acetate (200 mL), water (50 mL), and brine (50 mL) were added, and the organic layer was collected. The organic components were extracted with ethyl acetate (3 × 80 mL), and the combined organic layers were washed with water (30 mL) and brine (30 mL), dried over anhydrous $MgSO_4$, and concentrated under reduced pressure to give the reduced alcohol, ethyl 3-bromolactate. The crude product was dissolved in ethyl ether (10 mL) and cooled to −78 °C in a dry ice/acetone bath to allow crystallization. The mixture was then filtered while cold. 1.72 g of the product was collected as a white solid (38% yield). FTIR (attenuated total reflectance (ATR) (solid), cm^{-1}): 3419, 3337 (O−H); 2991 (COO−H); 1737 (C═O); 1215, 1172, 1093 (C−O); 584 (C−Br). ^{1}H NMR (600 MHz, D_2O): δ 4.57 (t, J = 3.8 Hz, 1H), 4.17−4.10 (m, 2H), 3.72−3.65 (m, 1H), 3.59 (dd, J = 11.1, 3.5 Hz, 1H), 1.15 (t, J = 7.2 Hz, 3H) (Figure S1). HRMS (+ESI): calculated for $C_{10}H_{16}O_6{}^{79}Br^{81}BrNa$ $[2M - 2H + Na]^+$ 414.9185, found 414.9188. MP: 43.8−45.2 °C.

Synthesis of Aqueous BiClLac. 3-Chlorolactic acid (83.01 mg, 0.667 mmol, 4.00 equiv) was placed in a 50 mL volumetric flask and dissolved by adding a portion of water. Bismuth nitrate pentahydrate (80.85 mg, 0.167 mmol, 1.00 equiv) was added and mixed with vortexing and sonication. The flask was filled to the mark with water and thoroughly mixed (Scheme 1). Haziness was observed when the ligand:bismuth nitrate pentahydrate ratio was less than 4:1, so any haziness was treated by adding a slight excess of 3-chlorolactic acid and mixing. The solution could be further purified by filtering to remove any unreacted bismuth compounds which could cause heterogeneous nucleation. FTIR (ATR (solid), cm^{-1}): 3414 (O−H); 2966 (COO−H); 1619 (C═O), 1333, 1184, 1086 (C−O); 640 (C−Cl). ^{1}H NMR (500 MHz, D_2O): δ 4.81 (dd, J = 4.3, 3.2 Hz, 1H), 3.87 (dd, J = 11.9, 4.3 Hz, 1H), 3.77 (dd, J = 11.9, 3.2 Hz, 1H)

https://doi.org/10.1021/acs.inorgchem.3c01114
Inorg. Chem. 2023, 62, 9640−9648

(Figure S1). ^{13}C NMR (126 MHz, D_2O): δ 177.22, 71.34, 47.17 (Figure S2).

Synthesis of Aqueous BiBrLac. The synthesis of BiBrLac was similar to that of BiClLac except using ethyl 3-bromolactate (131.35 mg, 0.667 mmol, 4.00 equiv) in place of 3-chlorolactic acid and including 10 mL of 3 M HNO_3 after adding ethyl 3-bromolactate but before adding bismuth nitrate pentahydrate. This step serves to hydrolyze the ester into an acid for complexation and improves overall solubility (Scheme 1). FTIR (ATR (solid), cm^{-1}): 3030 (COO−H); 1622 (C═O); 1325, 1170, 1092 (C−O); 646 (C−Br). ^{1}H NMR (500 MHz, D_2O): δ 4.63 (t, J = 3.8 Hz, 1H), 4.19 (m, 2H), 3.79−3.70 (m, 1H), 3.68−3.52 (m, 1H), 1.21 (t, J = 7.1 Hz, 3H) (Figure S1). ^{13}C NMR (126 MHz, D_2O): δ 172.77, 69.82, 62.87, 34.64, 13.28 (Figure S2).

Synthesis of Solid BiXLac. Solid BiXLac was achieved by evaporating the above solutions of BiClLac or BiBrLac under vacuum without the addition of heat. Smaller volumes of liquids can be used to lessen the time to evaporate. BiClLac was a white, crystalline solid, while BiBrLac was a white, hygroscopic solid.

Synthesis of Colloidal BiOX from Aqueous BiXLac. An aqueous solution of BiXLac was placed in a round-bottom flask equipped with a condenser. The flask was lowered into an oil bath held at 80 °C for either 14 h (BiClLac) or 2 h (BiBrLac) (Scheme 1). The BiOX particles were collected by centrifugation and washed with water.

Synthesis of BiOX via Solid-State Decomposition of Solid BiXLac. Solid BiXLac was heated in an oven for 2 h at 260 °C.

Synthesis of BiOX Films from Aqueous BiXLac. An aqueous solution of BiXLac was placed in an airbrush spray gun (7 cm^3 cup, 0.3 mm gravity-fed nozzle, connected to compressed air). A glass slide was placed on an aluminum block which had a thermocouple inside. The Al block was placed on a hot plate connected to a temperature controller set at 300 °C (the surface temperature is likely slightly lower). The solution was sprayed downward at a distance of 5 cm between the nozzle and the glass slide. A diagram of this apparatus is provided in Figure S3. The solution sprayed at a rate of 4.1 mL/min. Small amounts were sprayed onto the preheated glass slide, moving the airbrush to spray all regions of the slide evenly with one coat. The spray reacted on the heated surface until fully dry before more solution was sprayed. The thickness of the film could be controlled by the amount of solution sprayed. The glass slide with film was then placed in an oven to anneal at 200 °C for 12 h (BiClLac) or 2 h (BiBrLac).

Single-Crystal X-ray Diffraction (SCXRD). Suitable crystals for SCXRD were obtained by slow evaporation from aqueous solution. Experiments were conducted on a Bruker Venture D8 diffractometer equipped with a PhotonIII detector. Further details are provided in the Supporting Information.

Powder X-ray Diffraction (pXRD). pXRD data were collected with a PANalytical Empyrean instrument equipped with Cu Kα radiation (1.54178 Å) and an X'Celerator linear strip detector. An accelerating voltage of 45 kV and 40 mA current was used for all measurements. Scanning was from 5 to 80° 2θ, with a step size of 0.0167° 2θ. Powders were measured on a zero-background rotating silicon holder, except for temperature studies, which used a rotating aluminum holder to protect against Si cracking under thermal shock. Films were measured directly on the glass slides. Temperature studies on solid BiXLac were conducted by heating in an oven for 40 min followed by collecting pXRD patterns. The samples were then returned to the oven for another 40 min at the next higher temperature, repeating until all data points were collected.

Scanning Electron Microscopy (SEM). SEM images were obtained using a FEI Quanta 600 FEG microscope, operating at 30 kV with a spot size of 3, that interfaces with an Oxford INCA detector for energy-dispersive X-ray spectroscopy (EDS) analysis.

Nuclear Magnetic Resonance (NMR) Spectroscopy. ^{1}H and ^{13}C NMR spectra were recorded at room temperature on a Bruker 500 MHz Avance Neo (500 MHz for ^{1}H, 126 MHz for ^{13}C) spectrometer. Chemical shifts are reported in parts per million from tetramethylsilane, with the residual solvent resonance as the internal standard (D_2O: δ 4.79 ppm). Data are reported as follows: chemical shift, multiplicity (s = singlet, d = doublet, t = triplet, q = quartet, dd = doublet of doublets, br = broad, m = multiplet), coupling constants (Hz), and integration.

Fourier-Transform Infrared (FTIR) Spectroscopy. Infrared (IR) spectra were recorded on a Bruker Tensor II FTIR spectrometer with an attenuated total reflectance accessory collecting 16 scans at a resolution of 2 cm^{-1}.

X-ray Photoelectron Spectroscopy (XPS). The XPS experiments were carried out using PHI *VersaProbe* II instrument equipped with a focused monochromatic Al Kα source. The instrument base pressure was ca. 8×10^{-10} Torr. An X-ray power of 25 W at 15 kV was used for XPS spectra acquisition mode with a 100 μm beam size at the takeoff angles of 45° and normal X-ray incidence. The instrument work function was calibrated to give a binding energy (BE) of 84.0 eV for the Au $4f_{7/2}$ line for metallic gold, and the spectrometer dispersion was adjusted to give BEs of 284.8, 932.7, and 368.3 eV for the C 1s line of adventitious (aliphatic) carbon presented on the nonsputtered samples and Cu $2p_{3/2}$ and Ag $3d_{5/2}$ photoemission lines, respectively. The PHI dual charge neutralization system was used on all samples. The high-resolution Bi 4f and C 1s spectra were taken with a minimum of 10−60 s scans using 0.1 eV steps and 23.5 eV pass energy. All XPS spectra were recorded using PHI software *SmartSoft − XPS* v2.6.3.4 and processed using PHI *MultiPack* v9.3.0.3 and/or *CasaXPS* v.2.3.14 using Shirley background.

High-Resolution Mass Spectrometry (HRMS). Spectra were collected on a Thermo Scientific LTQ-Orbitrap XL mass spectrometer operating in +ESI mode. A small amount of crystals was added to 200 μL of methanol to dissolve the sample. 5 μL of this solution was added to 750 μL of a methanol solution, mixed, and used for testing.

Thermal Analysis. Thermogravimetric analysis (TGA) and differential scanning calorimetry (DSC) were performed on a Setram Labsys evo STA 1600 instrument using alumina crucibles under a simulated air atmosphere (4:1 Ar:O_2) while heating at 3 K/min from 25 to 650 °C. The evolved gases from the DSC/TGA instrument were analyzed by a Hiden QGA mass spectrometer (MS).

Melting Point. Melting points were determined on a Stanford Research Systems DigiMelt MPA 160 using glass capillaries and heating at 5.0 °C/min.

RESULTS AND DISCUSSION

Precursor Crystal Structures and Characterization. Crystal structures of BiClLac and BiBrLac are depicted in Figure 1 and Figures S4 and S5. A summary of the crystallographic data can be found in Table 1, and further details are given in the Supporting Information. BiClLac was formed by combining 3-chlorolactic acid and bismuth nitrate in a a 4:1 ratio (a slightly greater than 4:1 ratio ensures complete complexation). BiBrLac was made similarly, using ethyl 3-bromolactate. The ethyl functionality improved the stability of the ligand and was synthetically simpler and was ultimately removed by acid hydrolysis to achieve the BiBrLac structure. Creation of an iodo analog, "BiILac", was attempted using 3-iodolactic acid, but complexation was not observed likely due to iodide being a better leaving group, forming a solid at room temperature. With tailored ligand design and cold temperatures, we hypothesize BiILac would be obtainable and perform similarly.

The complexes are isostructural and crystallize in the monoclinic space group $C2/c$ (No. 15). The structures have a central bismuth atom with four ligands in a paddlewheel-like arrangement with the halogens farthest from the bismuth center. The ligands coordinate in a bidentate manner via a carboxylate oxygen and the hydroxide oxygen.[46−48] Bismuth has a coordination number of 8 in a slightly distorted square

https://doi.org/10.1021/acs.inorgchem.3c01114
Inorg. Chem. 2023, 62, 9640−9648

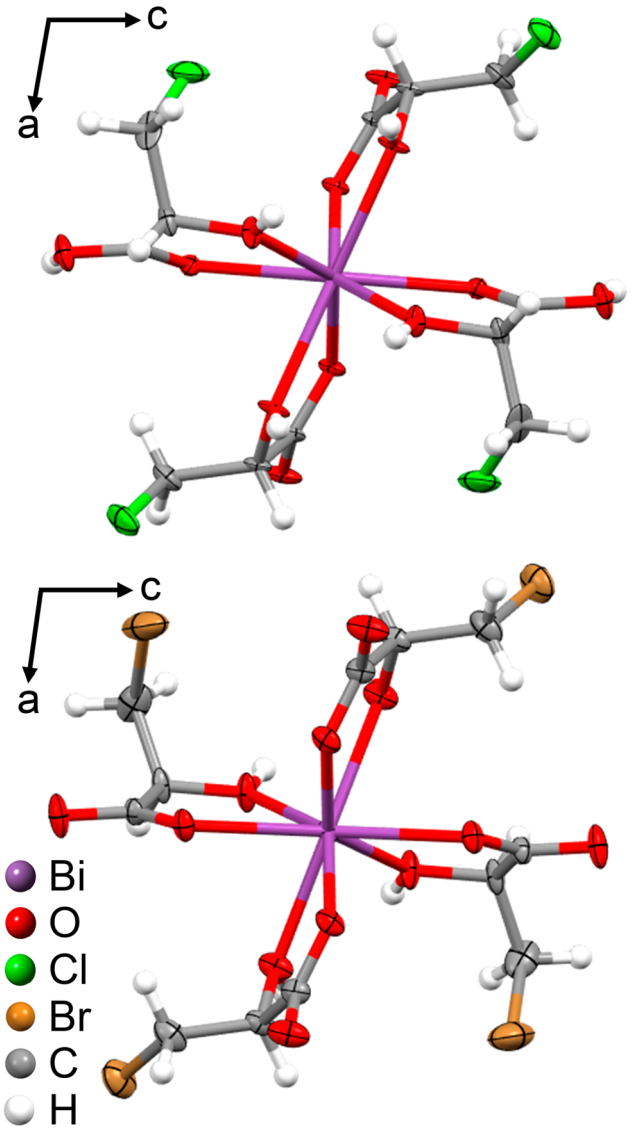

Figure 1. Crystal structures of BiClLac and BiBrLac viewed along the *b* axis. Ellipsoids are shown at the 50% probability level and hydrogens are shown as small spheres. Disorder is removed for clarity. Structures with atoms labeled can be found in Figure S4.

antiprismatic geometry (D_{4d}), determined by using SHAPE v2.1,[49] shape measure *S*,[50,51] and the bond angle method developed by Haigh[52] (Figure S6 and Table S1). Bismuth–oxygen bond distances range from 2.333(2) to 2.478(3) Å with a bite angle between 65.13(8) and 66.08(8)°. To maintain charge balance in the solid state, 3 of the 4 ligands are deprotonated at the acidic hydrogen position. To account for charge in the crystal structures (which have a C_2 symmetry element), the occupancy on one hydrogen in the asymmetric unit was set to 0.5.

While the solid-state crystal structures may differ slightly from the species in aqueous solution including potential diastereomers, the structures are reasonable and capture the ligation of bismuth causing its aqueous solubility. Note: under similar crystallization conditions, a bismuth chlorolactate dimer complex "BiClLacDimer" was also found but contains polymeric chains of bismuth and lactate repeating (Figures S5 and S7–S9 and Table S2). Because such a structure is unlikely in aqueous solution and the characterization presented below, we consider the aqueous structure of BiClLac to be that shown in Figure 1. The crystal details of this dimer structure are included in the Supporting Information for completeness and for the benefit of the crystal database literature.

Table 1. Crystallographic Data for BiXLac SSPs

	BiClLac	BiBrLac
formula	$C_{12}H_{17}BiCl_4O_{12}$	$C_{12}H_{17}BiBr_4O_{12}$
M_r	704.03	881.88
cryst syst	monoclinic	monoclinic
space group	*C*2/*c* (No. 15)	*C*2/*c* (No. 15)
a (Å)	19.6350 (6)	19.9244 (8)
b (Å)	5.7545 (1)	5.7442 (2)
c (Å)	19.2245 (6)	19.4012 (6)
β (deg)	100.4659 (11)	98.285 (2)
V (Å^3)	2136.03 (10)	2197.29 (14)
Z	4	4
$R(F^2 > 2\sigma(F^2))$	0.021	0.028
$R_w(F^2)$	0.053	0.063
S	1.11	1.08
T (K)	133	153
λ (Å)	0.71073	0.71073
D_{calcd} (g/cm^3)	2.189	2.666
μ (mm^{-1})	8.81	15.35

BiClLac and BiBrLac SSPs were characterized as aqueous solutions and as solid reagents by crystallizing from aqueous solution via slow evaporation. PXRD of the solid reagents shows their crystal phases match the calculated patterns from the SCXRD results (Figures S10 and S11). ^{1}H and ^{13}C NMR of the complexes in D_2O show full conversion from unbound ligands upon formation of the complexes and give the expected spectra (Figures S1 and S2, respectively). FTIR spectra of the ligands and BiXLac complexes as solids and in aqueous solution show the changes in vibrational frequencies of the ligands upon coordination to bismuth (Figure 2). This feature is best highlighted in the solid state, where the carboxylic acid or ester C═O stretch of the solid unbound ligands at ∼1740

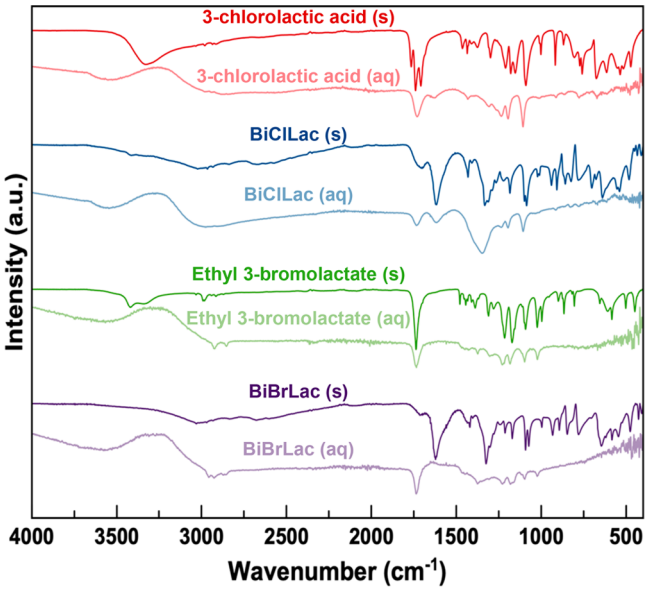

Figure 2. ATR-FTIR spectra of ligands and Bi-ligand complexes as solids and in aqueous solution.

https://doi.org/10.1021/acs.inorgchem.3c01114
Inorg. Chem. 2023, 62, 9640–9648

cm^{-1} is shifted to ~1620 cm^{-1} upon complexation as the C═O stretch weakens due to the Bi−O interaction in BiXLac.

Thermal analysis using combined TGA/DSC/MS highlights the decomposition of the ligands and bismuth-ligand complexes (Figures S12−S15). The thermal profile of 3-chlorolactic acid shows an endothermic peak at 82 °C from melting with most of the sample mass lost by 250 °C to H_2O, CO, and CO_2 as gaseous byproducts. Ethyl 3-bromolactate shows a similar profile although at lower temperatures, with melting at 46 °C and most of the mass lost by 175 °C. BiClLac shows a more complex thermal profile, with a more gradual loss in mass from 150 to 500 °C. Multiple sequential mass loss regions can be observed: 190 °C with evolution of H_2O and CO_2, 225 °C with evolution of H_2O, CO, and CO_2, 400 °C with evolution of CO and CO_2, and 490 °C with evolution of CO_2. Using the TGA/DSC/MS results alone, there is no clear region where BiOCl formation can be observed (theoretically at 37% mass remaining). This percent of mass remaining is reached around 400 °C, which coincides with an exothermic peak and mass loss region as CO and CO_2 evolve from the carbonaceous residue. We will compare the TGA/DSC/MS plots with the heated XRD experiments, presented in detail later.

Precursor Applications. With knowledge of the precursors, they were then used as SSPs to produce BiOX (Scheme 1). The SSPs are employed in three ways to demonstrate their utility and versatility. First, the aqueous precursors are heated to generate colloidal BiOX particles. Second, the dried precursors as solids can be heated to decompose into BiOX. Third, the aqueous SSPs can be sprayed onto a heated substrate (spray pyrolysis) to form films. For each of the three methods, pXRD showing pure phase BiOX and SEM images of the synthesized particles will be shown.

For an initial demonstration of these precursors, colloidal BiOX particles were synthesized from aqueous solution. BiOX materials are often synthesized by precipitation from aqueous solution, such as using $Bi(NO_3)_3{\cdot}5H_2O$ and NaCl. The immediate precipitation of the product results in a lack of effective tools to influence the product morphology. Using BiXLac as SSPs, the nucleation and growth rates are controlled by the addition of heat. BiOCl was synthesized by heating the aqueous BiClLac SSP in a round-bottom flask placed in an oil bath at 80 °C for 14 h, generating a powder comprised of nanoplates 100 nm to 1.5 μm across with thicknesses of less than 100 nm (Figure 3). BiOBr was similarly synthesized by heating BiBrLac at 80 °C for 2 h, resulting in larger 1.5−2.5 μm diameter spheres composed of intersecting nanoplates 100−500 nm across and thicknesses of less than 100 nm. The shorter time for BiBrLac reflects that bromide is a better leaving group than chloride, thus requiring less heat or time. Note that further structural control is anticipated with optimization of the reaction time and temperature and through the addition of structure-directing agents.

Moving from aqueous colloidal synthesis, the solid precursors were heated to decompose into BiOX. Samples of crystalline precursors were heated in an oven with periodic pXRD patterns being collected between heatings. Figure 4 and Figures S16 and S17 show the crystal phase of the crystalline BiClLac and BiBrLac precursors after heating at various temperatures. For BiClLac, the crystal phase of the precursor is maintained until 160 °C, where it becomes amorphous at 180 °C, and then shows peaks of BiOCl at 200 °C, which grow in

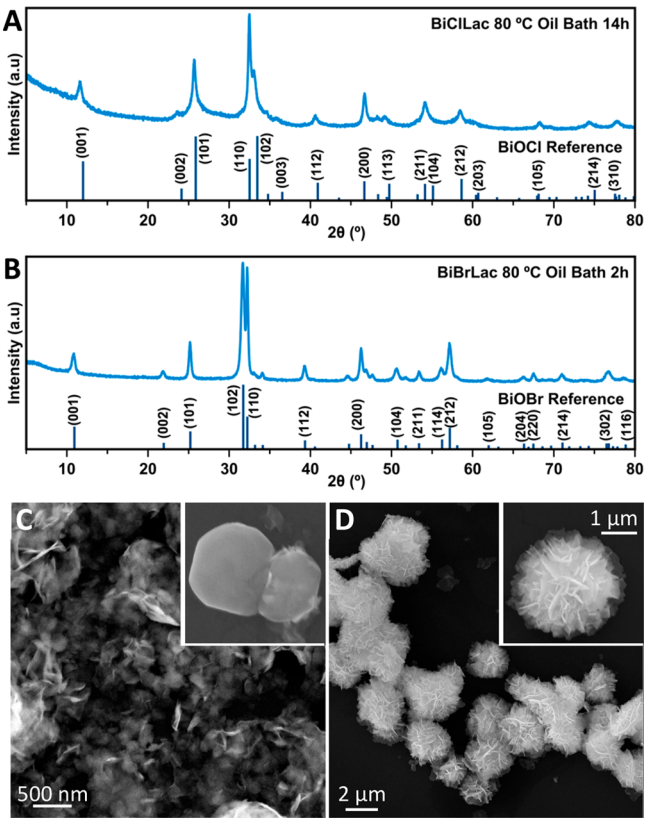

Figure 3. PXRD patterns (a, b) and SEM images (c, d) of BiOCl particles after aqueous colloidal synthesis in an 80 °C oil bath for 14 h (a, c) and BiOBr (b, d) particles after aqueous colloidal synthesis in an 80 °C oil bath for 2 h. BiOCl and BiOBr pXRD reference patterns are JCPDS 85-0861 and JCPDS 73-2061, respectively.

intensity for the rest of the heating (up to 260 °C). For BiBrLac, the crystal phase of the precursor is maintained until 140 °C, where it becomes amorphous from 160 to 220 °C, and then shows peaks of BiOBr at 240 and 260 °C. Comparing these findings with the TGA/DSC/MS plots (Figures S12 and S13), we can observe an endothermic valley followed by an exothermic peak for both precursors. The alignment of the temperatures of these regions with the XRD phase/temperature results indicates that the endothermic valley is caused by the precursor becoming amorphous, while the following exothermic peak represents the crystallization of BiOX.

SEM images of the room-temperature precursors show large precursor crystals which break down into much smaller BiOX particles after heating at 260 °C (0.5−2.5 μm across with thicknesses of less than 200 nm for BiOCl, and up to 1.5 μm across with thicknesses of less than 100 nm for BiOBr) (Figure 4b,c and Figure S16b,c). The TGA plot shows that BiClLac still has 81% of its initial mass at 200 °C, indicating that there is significant residue from the organic components still present (Figure S12). The pXRD data support the earlier claim of why there is no clear region in the TGA/DSC/MS plot where BiOCl forms.

Combining components of the previous two syntheses, spray pyrolysis was used as a method to synthesize BiOX films using the BiXLac SSPs. Film deposition of various materials has been explored previously using spray pyrolysis and related combustion syntheses, but this has mainly been applied to metal oxide and metal sulfide films.[53−59] An airbrush was used to spray the aqueous SSP solutions onto preheated glass slides

https://doi.org/10.1021/acs.inorgchem.3c01114
Inorg. Chem. 2023, 62, 9640−9648

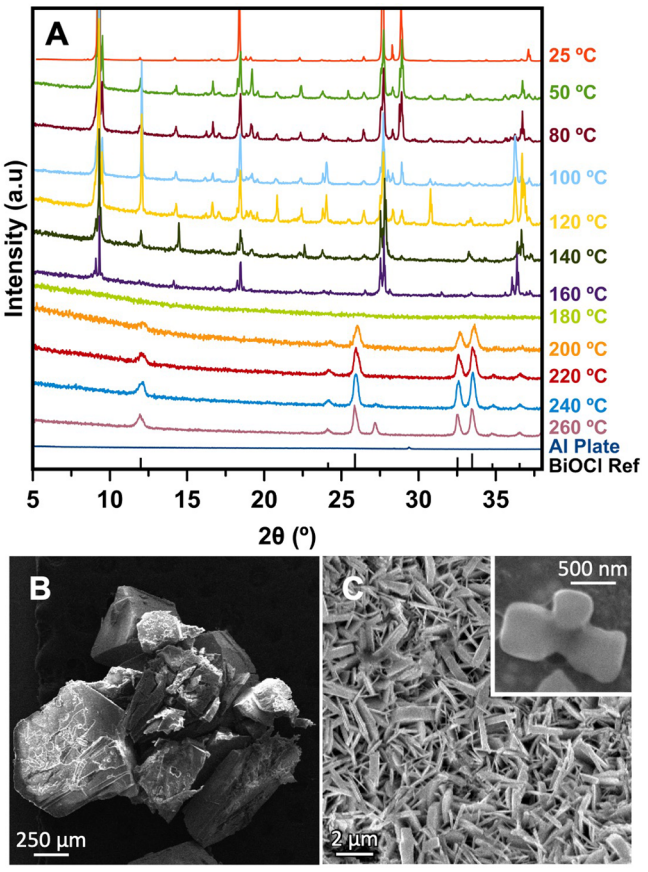

Figure 4. (a) PXRD patterns of BiClLac after heating at indicated temperatures. SEM images of BiClLac material at room temperature (b) and after heating to 260 °C (c). The inset in (c) is a single flat plate. The BiOCl pXRD reference pattern is JCPDS 85-0861.

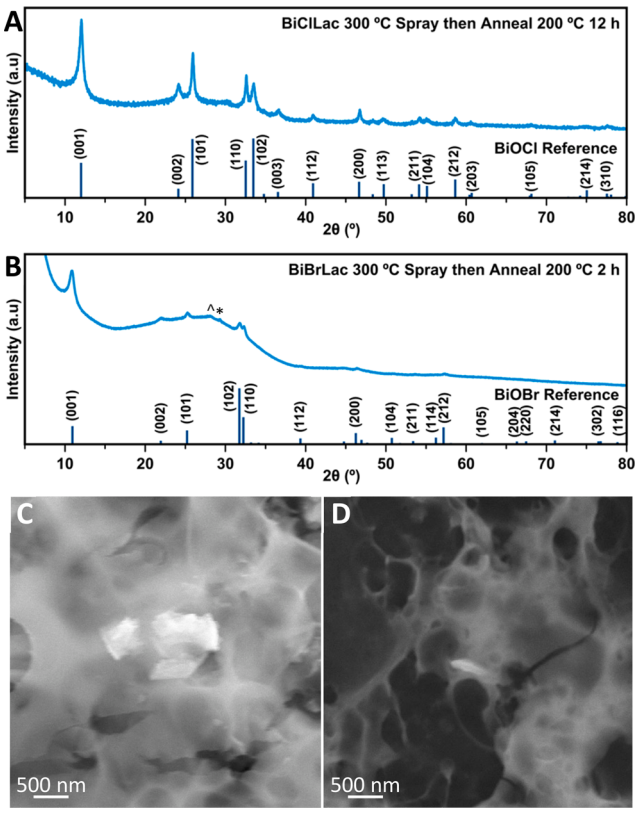

Figure 5. PXRD patterns (a, b) and SEM images (c, d) of BiOX films made by spraying BiXLac onto a glass slide at 300 °C and then annealing at 200 °C (BiClLac; annealed 12 h; a,c) or 2 h (BiBrLac; annealed 2 h; b, d). BiOCl and BiOBr pXRD reference patterns are JCPDS 85-0861 and JCPDS 73-2061, respectfully. ∧ and * represent minor phases of Bi_5O_7Br (JCPDS 76-9921) and $Bi_4O_5Br_2$ (JCPDS 71-3449), respectively.

on a heated block. After the solution is sprayed onto the glass slide, the heat from the slide triggers the reaction to make BiOX, much like with the colloidal aqueous synthesis. As the liquid evaporates, the organic residues further decompose as with solid-state decomposition. The fabrication of films can be advantageous to photocatalysis research, as their formation on conductive substrates enables photoelectrochemical cells.[60] Optimal conditions were found to be spraying the BiXLac aqueous solution onto glass slides held at 300 °C, followed by annealing in an oven at 200 °C for 12 h (BiClLac) or 2 h (BiBrLac). Immediately after spray pyrolysis, the film contains a mixture of partially decomposed reagents. PXRD of the as-sprayed films from BiBrLac shows weakly crystalline peaks of BiOBr with slight evidence of Bi_3O_4Br and Bi_5O_7Br impurity phases (Figure S18).

The as-sprayed BiCLac film showed BiOCl and Bi metal crystal phases (Figure S19), while the Bi 4f XPS region showed the presence of Bi^{3+} and additional signals from reduced oxidation states of Bi (Figure S20).[27,61] This caused some films to appear black. Such reduction of Bi^{3+} to Bi metal is a known phenomenon, having been reported in the literature as well.[62−64] We attribute the presence of Bi metal to carbothermal reactions where the carbonaceous residue char is oxidized by Bi^{3+} reducing to Bi^0. Despite this initial impurity, upon annealing in air at 200 °C, the Bi metal is reoxidized and is incorporated into phase-pure BiOX. Figure 5 and Figures S21−S24 show BiOCl and BiOBr films made using this process; the BiOCl film is well-crystallized as shown by pXRD, while the BiOBr film has an amorphous background and small Bi_3O_4Br and Bi_5O_7Br impurity phases. 2 h of annealing was used to form BiOBr, as this amount of time increased the BiOBr content without increasing the content of the impurity phases. While full optimization of the film deposition conditions was not studied, we demonstrate that BiOX films can be successfully deposited using a basic and inexpensive spray system and simple SSPs.

CONCLUSION

Here we have demonstrated two novel SSPs, BiClLac and BiBrLac, for the controlled aqueous synthesis of BiOCl and BiOBr, respectively. They have each been demonstrated in the synthesis of BiOX in three ways: aqueous colloidal synthesis, solid-state decomposition, and film formation by spray pyrolysis. These applications highlight the utility of these precursors across synthetic methods. These precursors expand the opportunities for bismuth chemistry in water, but more significantly, they provide an elegant solution to the challenge of controlled aqueous synthesis of bismuth oxyhalides: their fast nucleation and growth rates. By regulating the rate of halide ion formation through controlled application of heat, the nucleation and growth rates of bismuth oxyhalide materials is slowed during synthesis. With slowed nucleation and growth rates, we give time for further exploitation of faceting, shape control, and hierarchical design in bismuth oxyhalide systems.

https://doi.org/10.1021/acs.inorgchem.3c01114
Inorg. Chem. 2023, 62, 9640−9648

■ ASSOCIATED CONTENT

Supporting Information

The Supporting Information is available free of charge at https://pubs.acs.org/doi/10.1021/acs.inorgchem.3c01114.

NMR spectra and TGA/DSC/MS data of ligands and complexes, diagram of the spray pyrolysis apparatus, atom-labeled crystal structure representations and packing, additional pXRD, SEM-EDS, and XPS characterizations of materials, coordination geometry calculations, and crystal structure reports (PDF)

Accession Codes

CCDC 2211243, 2211246, and 2211249 contain the supplementary crystallographic data for this paper. These data can be obtained free of charge via www.ccdc.cam.ac.uk/data_request/cif, or by emailing data_request@ccdc.cam.ac.uk, or by contacting The Cambridge Crystallographic Data Centre, 12 Union Road, Cambridge CB2 1EZ, UK; fax: +44 1223 336033.

■ AUTHOR INFORMATION

Corresponding Author

Sara E. Skrabalak − *Department of Chemistry, Indiana University, Bloomington, Indiana 47405, United States;* orcid.org/0000-0002-1873-100X; Email: sskrabal@indiana.edu

Authors

Matthew N. Gordon − *Department of Chemistry, Indiana University, Bloomington, Indiana 47405, United States;* orcid.org/0000-0001-7212-9047

Yanyao Liu − *Department of Chemistry, Indiana University, Bloomington, Indiana 47405, United States*

M. Kevin Brown − *Department of Chemistry, Indiana University, Bloomington, Indiana 47405, United States;* orcid.org/0000-0002-4993-0917

Complete contact information is available at: https://pubs.acs.org/10.1021/acs.inorgchem.3c01114

Author Contributions

The manuscript was written through contributions of all authors. All authors have given approval to the final version of the manuscript.

Funding

This work was supported by Indiana University, US NSF DMR-2113536, Major Scientific Research Equipment Fund from the President of Indiana University and the Office of the Vice President for Research (award to Dr. Maren Pink for single-crystal XRD), and NSF Grant CRIF CHE-1048613 (powder XRD). Access to XPS at the Nanoscale Characterization Facility was provided by the NSF Award DMR MRI-1126394.

Notes

The authors declare no competing financial interest.

■ ACKNOWLEDGMENTS

M.N.G. thanks Dr. Maren Pink and Dr. Veronica Carta for useful crystallographic discussions and Dr. Kaustav Chatterjee, Jack Googasian, Megan Knobeloch, Dr. Daniel Beckett, Caleb Huizenga, Dr. Bin Feng, Dr. Duleeka Wannipurage, and Sheyda Partovi for fruitful scientific conversations. M.N.G. thanks Dr. Elisa Fatila for help with the shape measurement parameters, Dr. Yaroslav Losovyj for XPS support, and Quintin Brown for film characterization support. The authors thank the IU Molecular Structure Center, IU Nanoscale Characterization Facility, IU NMR Facility, Dr. Stephen Jacobson, and Dr. David Williams for access to instrumentation and training.

■ REFERENCES

(1) *The Future of Hydrogen: Seizing today's opportunities*; International Energy Agency: 2019.

(2) Nocera, D. G. Solar Fuels and Solar Chemicals Industry. *Acc. Chem. Res.* **2017**, *50*, 616−619.

(3) Brandon, N. P.; Kurban, Z. Clean energy and the hydrogen economy. *Philos. Trans. R. Soc., A* **2017**, *375*, 20160400.

(4) Eljack, F.; Kazi, M.-K. Prospects and Challenges of Green Hydrogen Economy via Multi-Sector Global Symbiosis in Qatar. *Front. Sustain.* **2021**, *1*, 612762.

(5) Guy, K. W. A. The Hydrogen Economy. *Trans. Inst. Chem. Eng.* **2000**, *78*, 324−327.

(6) Rifkin, J. *The Hydrogen Economy: The Creation of the Worldwide Energy Web and the Redistribution of Power on Earth*; J. P. Tarcher/Putnam: 2002; pp 1−294.

(7) Rosen, M. A.; Koohi-Fayegh, S. The prospects for hydrogen as an energy carrier: an overview of hydrogen energy and hydrogen energy systems. *Energy Ecol. Environ.* **2016**, *1*, 10−29.

(8) Staffell, I.; Scamman, D.; Velazquez Abad, A.; Balcombe, P.; Dodds, P. E.; Ekins, P.; Shah, N.; Ward, K. R. The role of hydrogen and fuel cells in the global energy system. *Energy Environ. Sci.* **2019**, *12*, 463−491.

(9) van Renssen, S. The hydrogen solution? *Nat. Clim. Change* **2020**, *10*, 799−801.

(10) Wang, Q.; Domen, K. Particulate Photocatalysts for Light-Driven Water Splitting: Mechanisms, Challenges, and Design Strategies. *Chem. Rev.* **2020**, *120*, 919−985.

(11) Chatterjee, K.; Skrabalak, S. E. Durable Metal Heteroanionic Photocatalysts. *ACS Appl. Mater. Interfaces* **2021**, *13*, 36670−36678.

(12) Ye, L. BiOX (X = Cl, Br, and I) Photocatalysts. In *Semiconductor Photocatalysis*; InTech: 2016. DOI: 10.5772/62626

(13) Di, J.; Xia, J.; Li, H.; Guo, S.; Dai, S. Bismuth oxyhalide layered materials for energy and environmental applications. *Nano Energy* **2017**, *41*, 172−192.

(14) Li, J.; Yu, Y.; Zhang, L. Bismuth Oxyhalide Nanomaterials: Layered Structures Meet Photocatalysis. *Nanoscale* **2014**, *6*, 8473−8488.

(15) Bhachu, D. S.; Moniz, S. J. A.; Sathasivam, S.; Scanlon, D. O.; Walsh, A.; Bawaked, S. M.; Mokhtar, M.; Obaid, A. Y.; Parkin, I. P.; Tang, J.; Carmalt, C. J. Bismuth oxyhalides: synthesis, structure and photoelectrochemical activity. *Chem. Sci.* **2016**, *7*, 4832−4841.

(16) Cheng, H.; Huang, B.; Dai, Y. Engineering BiOX (X = Cl, Br, I) nanostructures for highly efficient photocatalytic applications. *Nanoscale* **2014**, *6*, 2009−2026.

(17) Gordon, M. N.; Chatterjee, K.; Christudas Beena, N.; Skrabalak, S. E. Sustainable Production of Layered Bismuth Oxyhalides for Photocatalytic H2 Production. *ACS Sustainable Chem. Eng.* **2022**, *10*, 15622−15641.

(18) Wang, L.; Wang, L.; Du, Y.; Xu, X.; Dou, S. X. Progress and perspectives of bismuth oxyhalides in catalytic applications. *Mater. Today Phys.* **2021**, *16*, 100294.

(19) Subramanian, Y.; Dhanasekaran, A.; Omeiza, L. A.; Somalu, M. R.; Azad, A. K. A Review on Heteroanionic-Based Materials for Photocatalysis Applications. *Catalysts* **2023**, *13*, 173.

(20) Armelao, L.; Bottaro, G.; Maccato, C.; Tondello, E. Bismuth oxychloride nanoflakes: interplay between composition-structure and optical properties. *Dalton Trans.* **2012**, *41*, 5480−5.

(21) Ascencio-Aguirre, F. M.; Bazán-Díaz, L.; Mendoza-Cruz, R.; Santana-Vázquez, M.; Ovalle-Encinia, O.; Gómez-Rodríguez, A.; Herrera-Becerra, R. Chemical synthesis and characterization of bismuth oxychloride BiOCl nanoparticles. *Appl. Phys. A: Solids Surf.* **2017**, *123*, 155.

(22) Chunfa, L.; Zhenxin, X.; Jianbai, Z.; Pinguoo, J. Hydrolysis Mechanism of Bismuth in Chlorine Salt System Calculated by Density Functional Method. *Rev. Chim.* **2020**, *71*, 178−193.
(23) Fu, S.-m.; Li, G.-s.; Wen, X.; Fan, C.-m.; Liu, J.-x.; Zhang, X.-c.; Li, R. Effect of calcination temperature on microstructure and photocatalytic activity of BiOX (X = Cl, Br). *Trans. Nonferrous Met. Soc. China* **2020**, *30*, 765−773.
(24) Xu, Y.; Shi, Z.; Zhang, L.; Brown, E. M.; Wu, A. Layered bismuth oxyhalide nanomaterials for highly efficient tumor photodynamic therapy. *Nanoscale* **2016**, *8*, 12715−12722.
(25) Henle, J.; Simon, P.; Frenzel, A.; Scholz, S.; Kaskel, S. Nanosized BiOX (X = Cl, Br, I) Particles Synthesized in Reverse Microemulsions. *Chem. Mater.* **2007**, *19*, 366−373.
(26) Li, Z.; Huang, G.; Liu, K.; Tang, X.; Peng, Q.; Huang, J.; Ao, M.; Zhang, G. Hierarchical BiOX (X = Cl, Br, I) microrods derived from Bismuth-MOFs: In situ synthesis, photocatalytic activity and mechanism. *J. Cleaner Prod.* **2020**, *272*, 122892.
(27) Lindsjö, M.; Fischer, A.; Kloo, L. Improvements of and Insights into the Isolation of Bismuth Polycations from Benzene Solution − Single-Crystal Structure Determinations of Bi8[GaCl4]2 and Bi5-[GaCl4]3. *Eur. J. Inorg. Chem.* **2005**, *2005*, 670−675.
(28) Janczak, J. Synthesis and characterisation of bismuth(III) phthalocyaninate complex: [BiPc]4[Bi6I11Cl11]. *J. Mol. Struct.* **2010**, *965*, 125−130.
(29) Whitmire, K. H. Bismuth: Inorganic Chemistry. *Encycl. Inorg. Bioinorg. Chem.* **2004**, 1−32.
(30) Daniels, C. L.; Mendivelso-Perez, D. L.; Rosales, B. A.; You, D.; Sahu, S.; Jones, J. S.; Smith, E. A.; Gabbai, F. P.; Vela, J. Heterobimetallic Single-Source Precursors: A Springboard to the Synthesis of Binary Intermetallics. *ACS Omega* **2019**, *4*, 5197−5203.
(31) Dhanapala, B. D.; Munasinghe, H. N.; Suescun, L.; Rabuffetti, F. A. Bimetallic Trifluoroacetates as Single-Source Precursors for Alkali-Manganese Fluoroperovskites. *Inorg. Chem.* **2017**, *56*, 13311−13320.
(32) Kollek, T.; Gruber, D.; Gehring, J.; Zimmermann, E.; Schmidt-Mende, L.; Polarz, S. Porous and shape-anisotropic single crystals of the semiconductor perovskite CH3NH3PbI3 from a single-source precursor. *Angew. Chem., Int. Ed. Engl.* **2015**, *54*, 1341−1346.
(33) Abdulwahab, K. O.; Malik, M. A.; O'Brien, P. Direct Synthesis of Water-Soluble Nickel Ferrite Nanoparticles (NiFe2O4) by the Thermolysis of a Single Source Precursor. *FUW Trends in Science & Technology Journal* **2022**, *7*, 324−327.
(34) Ould-Ely, T.; Thurston, J. H.; Whitmire, K. H. Heterobimetallic bismuth−transition metal coordination complexes as single-source molecular precursors for the formation of advanced oxide materials. *C. R. Chim.* **2005**, *8*, 1906−1921.
(35) Akram, R.; Akhtar, J.; Akhtar, M.; Malik, M. A.; Revaprasadu, N.; Khan, M. D.; Bhatti, M. H. Single-source route to chalcopyrite-type CuFeS2 and CuFeSe2 nanocrystals and their structural and optical studies. *J. Mater. Sci.: Mater. Electron.* **2022**, *33*, 24619−24630.
(36) Bulimestru, I.; Shova, S.; Popa, N.; Roussel, P.; Capet, F.; Vannier, R.-N.; Djelal, N.; Burylo, L.; Wignacourt, J.-P.; Gulea, A.; Whitmire, K. H. Aminopolycarboxylate Bismuth(III)-Based Heterometallic Compounds as Single-Source Molecular Precursors for Bi4V2O11 and Bi2CuO4Mixed Oxides. *Chem. Mater.* **2014**, *26*, 6092−6103.
(37) Daniels, C. L.; Knobeloch, M.; Yox, P.; Adamson, M. A. S.; Chen, Y.; Dorn, R. W.; Wu, H.; Zhou, G.; Fan, H.; Rossini, A. J.; Vela, J. Intermetallic Nanocatalysts from Heterobimetallic Group 10−14 Pyridine-2-thiolate Precursors. *Organometallics* **2020**, *39* (7), 1092−1104.
(38) Buhro, W. E. Progress in molecular precursors for electronic materials. *Adv. Mater. Opt. Electron.* **1996**, *6*, 175−184.
(39) Lu, H.; Wright, D. S.; Pike, S. D. The use of mixed-metal single source precursors for the synthesis of complex metal oxides. *Chem. Commun.* **2020**, *56*, 854−871.
(40) Hepp, A. F.; Harris, J. D.; Apblett, A. W.; Barron, A. R., Commercialization of single-source precursors: Applications, intellectual property, and technology transfer. In *Nanomaterials via Single-Source Precursors: Synthesis, Processing and Applications*, Apblett, A. W., Barron, A. R., Hepp, A. F., Eds.; Elsevier: 2022; pp 563−600.
(41) Trindade, T.; O'Brien, P.; Zhang, X.-m. Synthesis of CdS and CdSe Nanocrystallites Using a Novel Single-Molecule Precursors Approach. *Chem. Mater.* **1997**, *9*, 523−530.
(42) Cowley, A. H.; Jones, R. A. The Single-Source Precursor Concept. A Case Study of Gallium Arsenide. *Polyhedron* **1994**, *13*, 1149−1157.
(43) Gordon, M. N.; Chatterjee, K.; Lambright, A. L.; Bueno, S. L. A.; Skrabalak, S. E. Organohalide Precursors for the Continuous Production of Photocatalytic Bismuth Oxyhalide Nanoplates. *Inorg. Chem.* **2021**, *60*, 4218−4225.
(44) Gordon, M. N.; Liu, Y.; Shafei, I. H.; Brown, M. K.; Skrabalak, S. E. Crystal structures of three beta-halolactic acids: hydrogen bonding resulting in differing Z′. *Acta Crystallogr., Sect. C: Struct. Chem.* **2022**, *78*, 257−264.
(45) Nishimura, Y.; Cho, H. Synthesis of 4,6-Unsubstituted 2-Aminodihydropyrimidine-5-carboxylates through Sequential Staudinger/Aza-Wittig/Cyclization Reactions. *Synlett* **2015**, *26*, 233−237.
(46) Stavila, V.; Davidovich, R. L.; Gulea, A.; Whitmire, K. H. Bismuth(III) complexes with aminopolycarboxylate and polyaminopolycarboxylate ligands: Chemistry and structure. *Coord. Chem. Rev.* **2006**, *250*, 2782−2810.
(47) Wullens, H.; Tinant, B.; Declercq, J.-P.; Devillers, M. A new dodecanuclear bismuth polyaminocarboxylate complex with 2-hydroxy-1,3-diaminopropanetetraacetic acid. *Inorg. Chim. Acta* **2003**, *343*, 335−342.
(48) Wullens, H.; Bodart, N.; Devillers, M. New Bismuth(III), Lanthanum(III), Praseodymium (III), and Heterodinuclear Bi−La and Bi−Pr Complexes with Polyaminocarboxylate Ligands. *J. Solid State Chem.* **2002**, *167*, 494−507.
(49) Llunell, M.; Casanova, D.; Cirera, J.; Bofill, J. M.; Alemany, P.; Alvarez, S.; Pinsky, M.; Avnir, D. *SHAPE V2.1*; Universitat de Barcelona: 2013 (this program has been developed by the group of Prof. Alvarez at the Universitat de Barcelona and is available from the authors at llunell@qf.ub.es).
(50) Xu, J.; Radkov, E.; Ziegler, M.; Raymond, K. N. Plutonium(IV) Sequestration: Structural and Thermodynamic Evaluation of the Extraordinarily Stable Cerium(IV) Hydroxypyridinonate Complexes. *Inorg. Chem.* **2000**, *39*, 4156−4164.
(51) Fatila, E. M.; Maahs, A. C.; Hetherington, E. E.; Cooper, B. J.; Cooper, R. E.; Daanen, N. N.; Jennings, M.; Skrabalak, S. E.; Preuss, K. E. Stoichiometric control: 8- and 10-coordinate Ln(hfac)3(bpy) and Ln(hfac)3(bpy)2 complexes of the early lanthanides La-Sm. *Dalton Trans.* **2018**, *47*, 16232−16241.
(52) Haigh, C. W. A New Simple Criterion for Distinguishing the Types of Structures in Eight-Coordinate Complexes: The Pattern of Bond Angles. *Polyhedron* **1995**, *14*, 2871−2878.
(53) Al-Rasheedi, A.; Ansari, A. R.; Abdeldaim, A. M.; Aida, M. S. Growth of zinc oxide thin films using different precursor solutions by spray pyrolysis technique. *Eur. Phys. J. Plus* **2022**, *137*, 1371.
(54) Owoeye, V. A.; Adewinbi, S. A.; Salau, A. O.; Orelusi, A. N.; Adeoye, A. E.; Akindadelo, A. T. Effect of precursor concentration on stoichiometry and optical properties of spray pyrolyzed nanostructured NiO thin films. *Heliyon* **2023**, *9*, e13023.
(55) Astuti, Y.; Fauziyah, A.; Nurhayati, S.; Wulansari, A. D.; Andianingrum, R.; Hakim, A. R.; Bhadura, G. Synthesis of α-Bismuth oxide using solution combustion method and its photocatalytic properties. *IOP Conf. Ser.: Mater. Sci. Eng.* **2016**, *107*, 012006.
(56) Perednis, D. *Thin film deposition by spray pyrolysis and the application in solid oxide fuel cells*. Ph.D. Dissertation. Swiss Federal Institute of Technology: 2003.
(57) Aydin, E.; Sankir, M.; Sankir, N. D. Influence of silver incorporation on the structural, optical and electrical properties of spray pyrolyzed indium sulfide thin films. *J. Alloys Compd.* **2014**, *603*, 119−124.
(58) Patil, G. E.; Kajale, D. D.; Gaikwad, V. B.; Jain, G. H. Spray Pyrolysis Deposition of Nanostructured Tin Oxide Thin Films. *ISRN Nanotechnol.* **2012**, *2012*, 1−5.

https://doi.org/10.1021/acs.inorgchem.3c01114
Inorg. Chem. 2023, 62, 9640−9648

(59) Sankir, N. D.; Aydin, E.; Unver, H.; Uluer, E.; Parlak, M. Preparation and characterization of cost effective spray pyrolyzed absorber layer for thin film solar cells. *Sol. Energy* **2013**, *95*, 21−29.
(60) Luévano-Hipólito, E.; Torres-Alvarez, D. A.; Torres-Martínez, L. M. Flexible BiOI thin films photocatalysts toward renewable solar fuels production. *J. Environ. Chem. Eng.* **2023**, *11*, 109557.
(61) Bjerrum, N. J.; Boston, C. R.; Smith, G. P. Lower Oxidation States of Bismuth. Bi+ and [Bi5]3+ in Molten Salt Solutions. *Inorg. Chem.* **1967**, *6*, 1162−1172.
(62) Yu, Y.; Yang, Z.; Shang, Z.; Wang, X. One-step solution combustion synthesis of Bi/BiOCl nanosheets: Reaction mechanism and photocatalytic RhB degradation. *J. Phys. Chem. Solids* **2023**, *174*, 111172.
(63) Kelly, Z.; Ojebuoboh, F. Producing Bismuth Trioxide and Its Application in Fire Assaying. *JOM* **2002**, *54*, 42−45.
(64) Levêque, G.; Abanades, S. Thermodynamic and Kinetic Study of the Carbothermal Reduction of SnO2 for Solar Thermochemical Fuel Generation. *Energy Fuels* **2014**, *28*, 1396−1405.

https://doi.org/10.1021/acs.inorgchem.3c01114
Inorg. Chem. 2023, 62, 9640−9648